Journal of Materials Chemistry C

PAPER

View Article Online
View Journal | View Issue



Cite this: J. Mater. Chem. C, 2015, 3, 3336

# One-step femtosecond laser patterning of light-trapping structure on dye-sensitized solar cell photoelectrodes†

Xi Zhang,‡ Hewei Liu,‡ Xuezhen Huang and Hongrui Jiang*

Received 20th November 2014,
Accepted 11th February 2015

DOI: 10.1039/c4tc02657h

www.rsc.org/MaterialsC

Light-trapping patterns were constructed in $TiO_2$ photoelectrodes for dye-sensitized solar cells (DSSCs) by a one-step femtosecond laser structuring method that utilized ablation to create patterns at the surface of nanostructured $TiO_2$ films. As a result, much more light was trapped in the photoelectrodes. Grating and orthogonal-grid patterns were studied, and the light trapping performance was optimized through the adjustment of pattern spacing, which was easily realized in the laser ablation process. With a 5 μm-spacing orthogonal-grid pattern, DSSCs showed a highest photon-to-electron conversion efficiency of 9.32% under AM 1.5G, a 13.5% improvement compared to the same cell without laser ablation. This simple and universal laser ablation method could be used to process many kinds of nanomaterials, and could be applied for various devices with nanostructures.

## 1. Introduction

Light-trapping designs and structures inside solar cells can overcome the insufficient light harvesting of the absorbing layers owing to their limited thickness. Therefore they are effective in improving the photon-to-electron conversion efficiency ($\eta$), and have been extensively studied in recent years for different types of solar cells.[1–6] The light-trapping structures are generally patterned on the photoactive layers. The dye-sensitized solar cell (DSSC) is considered as a promising type of solar cell due to its low cost and high efficiency.[7–9] The research on enhancing the light absorption of DSSCs is thus always a topic of great interest. The introduction of large $TiO_2$ nanoparticles as scattering centers in the photoelectrode is a conventional method to improve the light absorption.[10,11] Other methods exist too, such as taking advantage of the plasmonic effect,[12–14] modifying the electrolyte,[15] and using photonic crystals.[16] Creating light-trapping structures in DSSCs *via* patterning could be more efficient.[17–21] However, different from conventional solar cells based on bulk materials, patterning on nanostructured $TiO_2$ for DSSCs is much more difficult. So far, there has been only one method, which is essentially through template molding, applied for the DSSCs based on printed $TiO_2$ photoelectrodes. Kim *et al.* first reported a nanopatterned $TiO_2$ photoelectrode for DSSCs *via* a polydimethylsiloxane (PDMS) nanostamp.[19] Wooh *et al.* fabricated pyramid-like structures *via* pressing a mold onto the top of a $TiO_2$ paste, and obtained high performance of the DSSCs.[20] Recently, Lee *et al.* patterned a grating structure on the bottom of a $TiO_2$ photoelectrode using a PDMS stamp.[21] Nevertheless, this method requires that the electrode materials be in a paste-like state for printing before solidification. It would be advantageous if the solidified $TiO_2$ photoelectrode could be directly patterned, eliminating the requirement on the state of the electrode material. There has been no report yet, though, on such one-step patterning on the nanostructured $TiO_2$ photoelectrode.

Femtosecond (fs) laser ablation has been proven a simple and effective method to create micro- or nano-structures directly onto the surface of bulk materials.[22–26] In this study, we utilized fs laser to directly ablate the surface of nanostructured $TiO_2$ film and obtain a periodic morphology for light-trapping. This one-step fabrication utilizing fs laser ablation is a cost-effective, versatile and environmentally friendly approach, and can form any patterns without photolithography and its intrinsically involved steps. More importantly, this universal method can be applied to many more categories of nanomaterials, and is not limited by the fabrication process of the devices or the states of the materials during the process. The sub-picosecond laser-matter interaction avoids thermal damages of the materials and substrates, and allows for fabrication of structures within a few micrometers.[27] The fs laser generates hierarchical structures combining both micro- and nano-scales in a single ablation;[28,29] such dual-scale micro-/nano-structure can increase the surface area of $TiO_2$.

*Materials Science Program, Department of Electrical and Computer Engineering, University of Wisconsin-Madison, Madison, WI, 53706, USA.*
*E-mail: hongruijiang@wisc.edu; Fax: +1-608-262-1267; Tel: +1-608-265-9418*

† Electronic supplementary information (ESI) available. See DOI: 10.1039/c4tc02657h

‡ X. Zhang and H. Liu contributed equally to this work.

A grating pattern and an orthogonal-grid pattern were adopted in this work and various size parameters of the patterns were investigated. The laser-ablated $TiO_2$ photoelectrode with 5 μm orthogonal-grid spacing demonstrated the strongest light-trapping effect. The corresponding fabricated DSSCs showed the highest $\eta$ of 9.32%, increased from 8.21% without laser ablation, indicating a 13.5% of improvement in $\eta$ due to laser patterning of the $TiO_2$ photoelectrode alone. This universal laser ablation method also has great potential for other types of nanostructured solar cells.

## 2. Experimental

10 μm-thick $TiO_2$ film consisting of 20 nm $TiO_2$ nanoparticles was deposited onto fluorine-doped tin oxide (FTO) glass (1.5 cm × 1.5 cm, TEC-15, MTI Co.) using a screen-printing method before being sintered at 500 °C. The area of the active region on the FTO glass was 0.12 $cm^2$, measured by a microscope (Olympus BX51M).

The vertical-polarized laser (Uranus2000-1030-1000, PolarOnyx) with a pulse duration of 700 fs, a wavelength of 1030 nm, and a repetition rate of 120 kHz was delivered into an objective lens (N.A. = 0.8, Nikon) and focused on the sample surface. The diameter of the focal spot was 1.5 μm. A mechanical shutter was used to turn the laser on and off. A neutral density attenuator and polarizer were used to control the power and polarization of the laser beam. The sample was mounted on a computer-controlled *xyz* stage (Newport XMS-160, XMS-100 and GTS-30V for the *x*-axis, *y*-axis and *z*-axis, respectively). By translating the sample, the microstructures were ablated by the focused laser pulses, and a CCD camera and relay lens were used for real-time monitoring of the ablation process. The laser energy was 40 nJ per pulse, and the scanning speed was 2 mm $s^{-1}$.

The ablated $TiO_2$ films with grating and orthogonal-grid patterns were then cleaned with deionized water before being coated with a 3 μm-thick scattering layer consisting of 50 nm $TiO_2$ nanoparticles using the same screen-printing method. The films were subsequently sintered again at 500 °C for 1 h. After being cooled down to 120 °C, they were soaked into the dye solutions (0.3 mM N719 in acetonitrile-*tert*-butanol, v/v = 1 : 1) and kept at room temperature for 24 h. The counter electrode was Pt-coated FTO glass with two drilled holes for filling the electrolyte. The Pt layer was deposited onto the FTO glass by an electrodeposition process in $H_2PtCl_6$ solution (0.5 M). A 25 μm-thick Surlyn (SOLARONIX, Switzerland) film was used as a spacer between the photoelectrode and the counter electrode for each DSSC. The redox electrolyte contained 0.1 M LiI, 0.05 M $I_2$, and 0.6 M 1,2-dimethyl-3-propylimidazolium iodide, using acetonitrile as solvent.

The morphology of the $TiO_2$ film surfaces was characterized by scanning electron microscopy (SEM, Zeiss LEO 1530). X-ray diffraction (XRD) spectra of $TiO_2$ films were recorded using a Bruker/Siemens Hi-Star 2d X-ray diffractometer with a monochromatic Cu K-alpha point source (0.8 mm). The optical transmittance and reflectance spectra of the $TiO_2$ photoelectrodes were recorded using an optical fiber detector (Edmund) equipped with an integrating sphere (Thorlabs). The *J*–*V* measurements of the DSSCs were performed using a Keithley 2400 source meter under the illumination of simulated AM 1.5G solar light (Oriel 94022A equipped with a 150 W Xe lamp and an AM 1.5G filter). For the incident photon-to-current efficiency (IPCE) measurement, $J_{sc}$ of DSSCs at each wavelength in the range of 400–700 nm was recorded by the Keithley 2400 source meter before the IPCE values were calculated. The light from the Oriel 94022A light source was conducted through a monochromator (Mini-Chrom 300–800 nm, Edmund Optics) and illuminated to the DSSCs. The wavelength step was set to 10 nm. The amount of adsorbed dye was determined from the absorbance of the desorbed dye solution at 510 nm using the same monochromator. The dye-loaded $TiO_2$ films were immersed in 0.1 M NaOH aqueous solution for 20 min for dye desorption. The transmittance spectra of the $TiO_2$ photoelectrodes with and without laser ablation were simulated by the software Zemax (Radiant Zemax).

## 3. Results and discussion

### 3.1. Patterning by laser ablation

The optical setup for structuring the $TiO_2$ thin film is shown in Fig. 1a. Linear polarized laser pulses were delivered into an objective lens and focused on the sample surface. A nanostructured $TiO_2$ photoelectrode before laser ablation was deposited onto a FTO glass substrate, followed by sintering at 500 °C. The thickness of the $TiO_2$ film was 10 μm, consisting of 20 nm nanoparticles. By scanning the laser beam along programmed paths, any pattern could be directly written onto the $TiO_2$ film without other processing. The pulse width was 700 fs, which is much shorter than the heat diffusion time between the lattice of $TiO_2$. Hence the thermal effect could hardly affect the porosity of the nanostructure $TiO_2$ film.[30] In the experiments, both grating and orthogonal-grid patterns were defined. The optical microscopic images of a grating and an orthogonal-grid pattern are shown in Fig. 1b and c, respectively. Both the grating and orthogonal-grid patterns had intervals between two grid lines ranging between 5 mm and 40 mm. The details of the structures are shown in the SEM image (Fig. 1d). The line width of the grids was about 2 μm, while the ablation depth was also about 2 μm. An interesting phenomenon is the formation of nanostructures in the laser irradiated regions, as shown in Fig. 1e. These structures can be categorized as the laser-induced periodic surface structures that were commonly observed after laser ablation and that were demonstrated to increase the surface area of the material.[28,29]

XRD measurements were performed to explore the potential change in $TiO_2$ induced by the laser ablation. Fig. 2 shows the XRD spectra of the $TiO_2$ film before and after laser ablation. All the peaks in the spectrum of the bare $TiO_2$ film are indexed to the standard anatase pattern. After laser ablation, the positions of all the peaks did not change and no extra peaks were observed. Therefore, the lattice of anatase $TiO_2$ nanoparticles was not modified by the laser ablation process, nor was any impurity or contamination introduced.

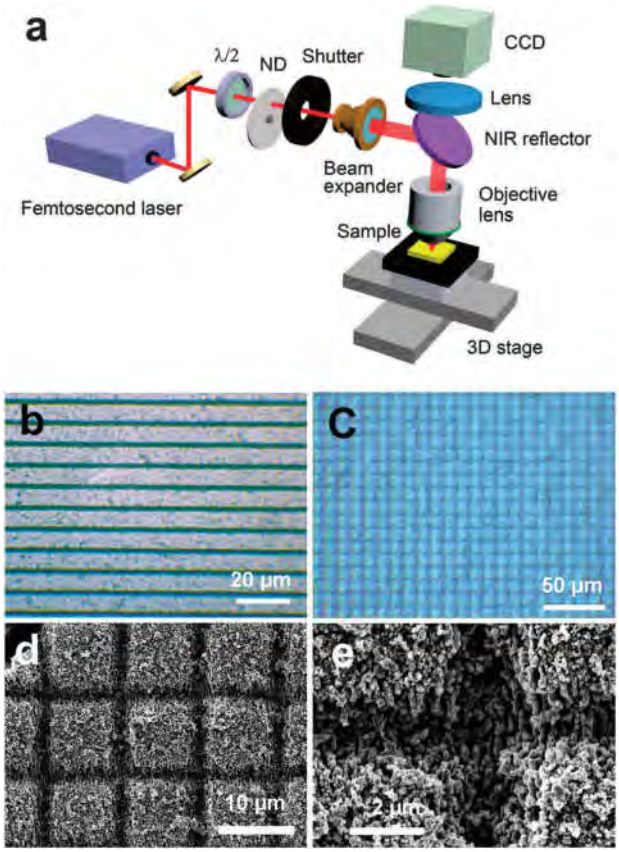


Fig. 1 (a) Schematic of the optical setup for the laser ablation structuring; (b) a grating pattern (10 μm grid spacing) of the laser-ablated nanostructured $TiO_2$ film; (c) an orthogonal-grid pattern (10 μm grid spacing) of the laser-ablated nanostructured $TiO_2$ film; (d) SEM image of the orthogonal-grid pattern; (e) enlarged image of (d): the formation of the nanostructures in the laser irradiated regions.

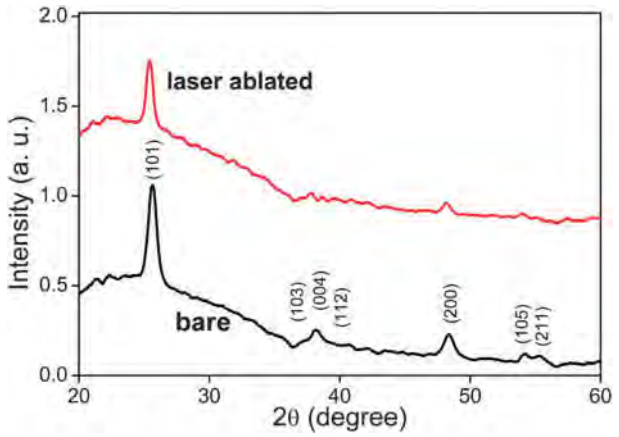


Fig. 2 XRD spectra of nanostructured $TiO_2$ film before and after laser ablation.

### 3.2. Light-trapping effect

After laser ablation, the 10 μm-thick $TiO_2$ film was covered with a 3 μm-thick scattering layer, which consisted of 50 nm $TiO_2$ particles. Fig. 3 shows the cross-sectional SEM images of the $TiO_2$ film with the orthogonal-grid structure covered by the scattering layer. The laser-ablated lines show sloped sidewalls

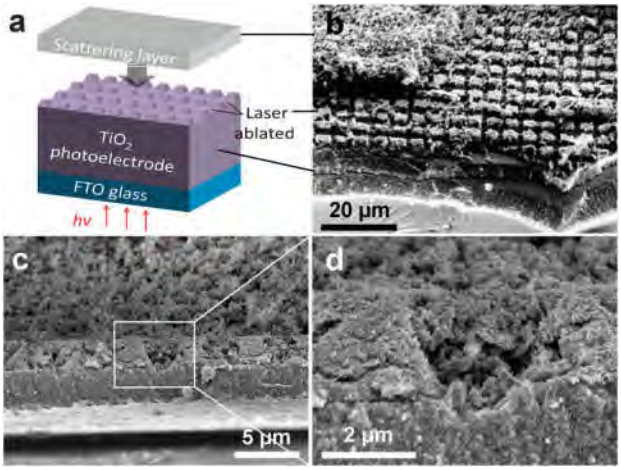


Fig. 3 (a) Schematic of the $TiO_2$ photoelectrode, which is patterned by laser ablation and covered by a scattering layer; (b), (c) cross-sectional SEM images of the $TiO_2$ film with an orthogonal-grid structure (5 μm grid spacing) covered by the scattering layer; (d) enlarged image of the selected region in (c).

with a height of 2 μm. Such sloped sidewalls benefit the reflection of light, thus the light trapping effect.[20] The cross-sectional profile and the depth of the laser-ablated structures can be changed by varying the focusing condition, the power, and the scanning speed of the laser.

In this study, four grid spacings of 5 μm, 10 μm, 15 μm, and 40 μm were used for both the grating and the orthogonal-grid patterns. In order to observe the effect of light-trapping by laser ablation, the transmittance spectra of the $TiO_2$ films without the scattering layer were recorded. Fig. 4 shows the results of the bare and the laser-ablated $TiO_2$ films with the same thickness of 10 μm. The reduced light transmittance after laser ablation indicates the enhanced light reflection plus absorption from the significantly increased surface area on top of the $TiO_2$ photoactive layer by laser ablation, which benefits the light harvesting of DSSCs. For each grid spacing, the grating pattern has a higher transmittance than that of the orthogonal-grid pattern, because the latter has a nearly doubled ablation area. As the grid spacing decreases, the reflected and scattered light increases owing to the increased density of the light trapping structure. Therefore, the transmittance decreases gradually. From Fig. 4, there was little reduction in transmittance when the grid spacing reached 40 μm. The reflectance spectra of the bare and laser-ablated $TiO_2$ films are shown in Fig. S1 (ESI†), where the reflectance is increased after laser ablation, and the orthogonal-grid pattern has a higher reflectance than that of the grating pattern. Fig. S2 (ESI†) shows the simulated transmittance spectra of the orthogonal-grid patterns, which are in agreement with the measured results.

### 3.3. Performance of DSSCs

After being covered with 3 μm-thick scattering layers, the bare and laser-ablated $TiO_2$ films were loaded with dyes before being assembled into DSSCs. The schematic of a final DSSC with an orthogonal-grid-patterned $TiO_2$ photoelectrode is shown in

 

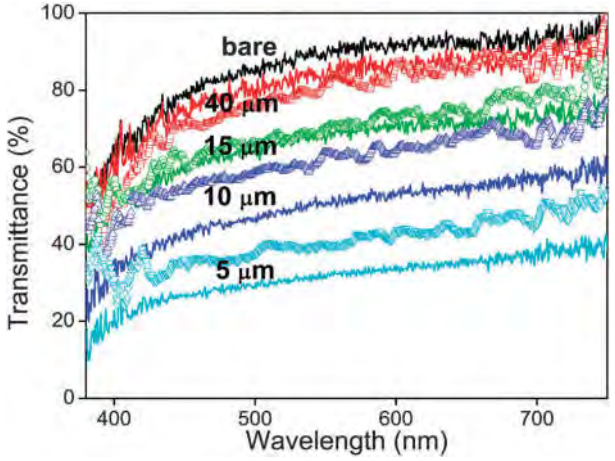


Fig. 4 Transmittance spectra of nanostructured $TiO_2$ films before and after laser ablation. The grid spacings of both the grating and the orthogonal-grid patterns on the ablated photoelectrodes are 5 μm (light blue curves), 10 μm (blue curves), 15 μm (green curves), and 40 μm (red curves), respectively. The black solid curve indicates the bare film. The colored solid curves indicate the films with the orthogonal-grid patterns. The colored scatter curves indicate the films with the grating patterns.

Fig. 5. The *J*–*V* results of all these DSSCs under simulated AM 1.5G illumination are shown in Fig. 6, and all the corresponding parameters are listed in Table 1. For the DSSCs with laser ablation, the grid spacings for each of the two patterns were also 5 μm, 10 μm, 15 μm, and 40 μm respectively. The width of laser-ablated line was kept the same at 2 μm. $\eta$ of the DSSC without laser ablation was 8.21%. The short-circuit photocurrent density ($J_{sc}$) was significantly improved after the photoelectrode was laser-ablated with the light-trapping grids, while the open-circuit voltage ($V_{oc}$) remained at about 0.7 V. The fill factor (FF) was reduced a little after laser ablation, but

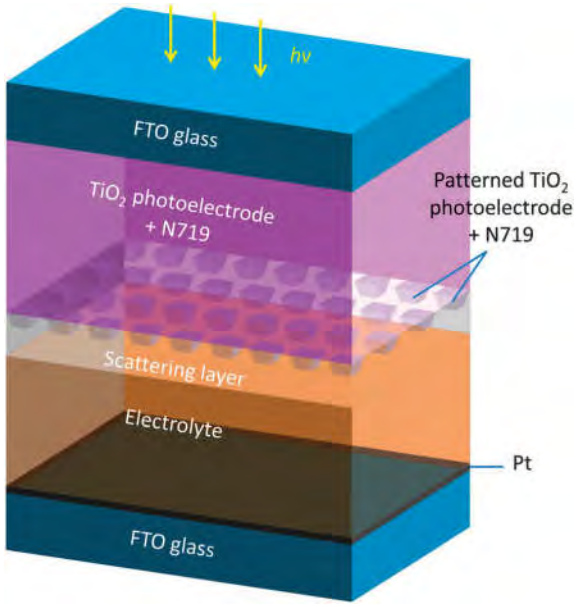


Fig. 5 Schematic of the DSSC with a patterned $TiO_2$ photoelectrode by laser ablation.

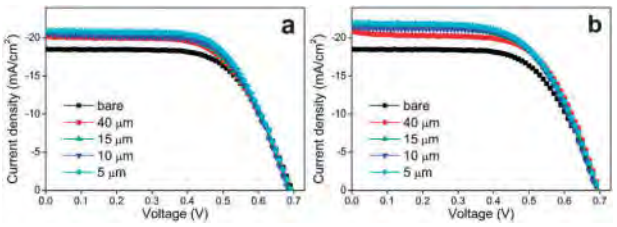


Fig. 6 *J*–*V* curves of the DSSCs using bare and laser-ablated $TiO_2$ photoelectrodes. (a) DSSCs with bare and grating-patterned $TiO_2$; (b) DSSCs with bare and orthogonal-grid-patterned $TiO_2$. The grid spacing of both types of patterns on the ablated photoelectrodes ranges from 5 μm to 40 μm.

Table 1 *J*–*V* parameters of all the DSSCs

| Pattern | $V_{oc}$ (V) | $J_{sc}$ (mA cm$^{-2}$) | FF (%) | $\eta$ (%) |
|---|---|---|---|---|
| Bare | 0.70 | 18.6 | 63.2 | 8.21 |
| 40 μm grating | 0.69 | 20.2 | 61.8 | 8.61 |
| 15 μm grating | 0.69 | 20.6 | 61.3 | 8.73 |
| 10 μm grating | 0.69 | 20.5 | 62.7 | 8.88 |
| 5 μm grating | 0.70 | 20.9 | 62.4 | 9.14 |
| 40 μm orthogonal | 0.70 | 20.9 | 62.6 | 9.16 |
| 15 μm orthogonal | 0.70 | 21.9 | 60.0 | 9.18 |
| 10 μm orthogonal | 0.69 | 21.6 | 61.8 | 9.23 |
| 5 μm orthogonal | 0.70 | 21.9 | 60.7 | 9.32 |

remained at almost the same level for different pattern parameters. $\eta$ for the four DSSCs with grating patterns ranges from 8.61% to 9.14%, while $\eta$ for the four DSSCs with orthogonal-grid patterns ranges from 9.16% to 9.32%, all of which are much higher in comparison with the cell without laser ablation. This indicates that the patterned light-trapping grids on the photoelectrode improve the light scattering effect, which in turn enhances the total light absorption of the cell. As mentioned before, the ablation depth was about 2 μm, which removed a small portion of the total 10 μm-thick dye-loaded $TiO_2$ layer. The laser ablation has a quite limited influence on the amount of the loaded dye molecules, and would not increase the dye amount. The measured amount of adsorbed dye on each $TiO_2$ films is shown in Table S1 (ESI†). The dye amount was reduced after laser ablation. Therefore, the performance enhancement is ascribed to the light-trapping effect. The improvement of $\eta$ is mainly attributed to the enhancement of $J_{sc}$. For either the grating pattern or the orthogonal-grid pattern with different spacings, the performance of DSSCs increases as the spacing decreases. As expected, the DSSC with the orthogonal-grid pattern has a better performance than that with the grating pattern at each given grid spacing. For both types of patterns, $J_{sc}$ is significantly improved from no ablation to 40 μm of spacing and then down to 15 μm of spacing. However, $J_{sc}$ remains almost at the same level from 15 μm of spacing to 5 μm of spacing for both types of patterns, although the transmittance kept decreasing as shown in Fig. 4. This implies that not all of the increased trapped light contributed to the ultimate photocurrent generation.

The results of the IPCE measurements from 400 nm to 750 nm are shown in Fig. 7. For each of the two pattern types,

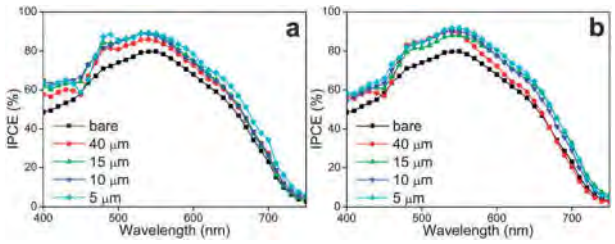


Fig. 7 IPCE spectra of the DSSCs using bare and laser-ablated $TiO_2$ photoelectrodes. (a) DSSCs with bare and grating-patterned $TiO_2$; (b) DSSCs with bare and orthogonal-grid-patterned $TiO_2$. The grid spacing of both types of patterns on the ablated photoelectrodes ranges from 5 μm to 40 μm.

the IPCE increases as the grid spacing decreases in the full range, which agrees well with the trend in $J_{sc}$. The IPCE improvement after the formation of the light-trapping structure covers almost all wavelengths measured. For the curves corresponding to 10 μm, 15 μm, 40 μm of spacing in Fig. 7a and 40 μm of spacing in Fig. 7b, the increase mainly lies in the wavelength range below 600 nm, which is quite different from the transmittance results in Fig. 4, where the increase almost covers the whole wavelength range. This indicates that the trapped light by the ablated patterns has a wavelength selectivity when absorbed by the dye. One of the reasons could be the dependence of the reflection angle on the wavelength. When the grid spacing of the grating pattern is reduced to 5 μm or the grid spacing of the orthogonal-grid pattern is reduced to 15 μm and less, the increase in IPCE above 600 nm becomes more significant. For the orthogonal-grid patterns, the IPCEs of the DSSCs with 5 μm, 10 μm, and 15 μm spacings are much greater than that with 40 μm spacing. This agrees with the variation in $J_{sc}$ with the same spacings. The ablated surface reflected more light back to the dye-loaded photoelectrode, and the photocurrent increased. The parameters of the laser-ablated pattern could influence the scattering of the light at different wavelengths, and a better matching with the absorption spectrum of the dye could result in better performance of DSSCs.

## 4. Conclusions

In conclusion, we utilized fs laser ablation to directly write grating and orthogonal-grid patterns as light-trapping structures on nanostructured $TiO_2$ films to enhance light harvesting in DSSCs. The fabricated DSSCs with the light-trapping structures on the photoelectrodes showed significantly improved performance. The parameters of the patterns could be easily adjusted in the laser ablation process. The grid spacing was varied to optimize the light trapping effect. The $TiO_2$ film with 5 μm orthogonal-grid spacing demonstrated the best light-trapping effect, and the corresponding DSSC presented the highest $\eta$ of 9.32%, which is a 13.5% improvement compared with the DSSC without laser ablation. This simple, single-step fs laser ablation process is universal and can be applied to processing of many kinds of nanomaterials for a host of applications. For example, it could be utilized to improve the light harvesting efficiency of a number of novel solar cells based on nanostructures. Another example would be the production of novel optical materials taking advantage of the dual-scale micro-/nano-structures. In the future, the wavelength selectivity of the patterns by laser ablation will be further investigated, and the detailed light-trapping mechanism will be explored.

## Acknowledgements

This work was supported by the US National Institute of Health (Grant No. 1DP2OD008678-01). This research utilized NSF supported shared facilities at the University of Wisconsin.

## Notes and references

1 E. Garnett and P. Yang, *Nano Lett.*, 2010, **10**, 1082.
2 H. A. Atwater and A. Polman, *Nat. Mater.*, 2010, **9**, 205.
3 C. Battaglia, J. Escarré, K. Söderström, L. Erni, L. Ding, G. Bugnon, A. Billet, M. Boccard, L. Barraud, S. D. Wolf, F.-J. Haug, M. Despeisse and C. Ballif, *Nano Lett.*, 2011, **11**, 661.
4 C. Battaglia, J. Escarré, K. Söderström, M. Charrière, F.-J. Haug, M. Despeisse and C. Ballif, *Nat. Photonics*, 2011, **5**, 535.
5 D. M. Callahan, J. N. Munday and H. A. Atwater, *Nano Lett.*, 2012, **12**, 214.
6 R. Betancur, P. Romero-Gomez, A. Martinez-Otero, X. Elias, M. Maymo and J. Martorell, *Nat. Photonics*, 2013, **7**, 995.
7 M. Grätzel, R. A. J. Janssen, D. B. Mitzi and E. H. Sargent, *Nature*, 2012, **488**, 304.
8 B. E. Hardin, H. J. Snaith and M. D. McGehee, *Nat. Photonics*, 2012, **6**, 162.
9 A. Yella, H. W. Lee, H. N. Tsao, C. Y. Yi, A. K. Chandiran, Md. K. Nazeeruddin, E. W. G. Diau, C. Y. Yeh, S. M. Zakeeruddin and M. Grätzel, *Science*, 2011, **334**, 629.
10 S. Hore, C. Vetter, R. Kern, H. Smit and A. Hinsch, *Sol. Energy Mater. Sol. Cells*, 2006, **90**, 1176.
11 F. Huang, D. Chen, X. L. Zhang, R. A. Caruso and Y.-B. Cheng, *Adv. Funct. Mater.*, 2010, **20**, 1301.
12 S. Guldin, S. Hüttner, M. Kolle, M. E. Welland, P. Müller-Buschbaum, R. H. Friend, U. Steiner and N. Tétreault, *Nano Lett.*, 2010, **10**, 2303.
13 A. Mihi, C. Zhang and P. V. Braun, *Angew. Chem., Int. Ed.*, 2011, **50**, 5712.
14 C. T. Yip, H. Huang, L. Zhou, K. Xie, Y. Wang, T. Feng, J. Li and W. Y. Tam, *Adv. Mater.*, 2011, **23**, 5624.
15 M. Wang, X. Pan, X. Fang, L. Guo, W. Liu, C. Zhang, Y. Huang, L. Hu and S. Dai, *Adv. Mater.*, 2010, **22**, 5526.
16 I.-K. Ding, J. Zhu, W. Cai, S.-J. Moon, N. Cai, P. Wang, S. M. Zakeeruddin, M. Grätzel, M. L. Brongersma, Y. Cui and M. D. McGehee, *Adv. Eng. Mater.*, 2011, **1**, 52.
17 F. Wang, N. K. Subbaiyan, Q. Wang, C. Rochford, G. Xu, R. Lu, A. Elliot, F. D'Souza, R. Hui and J. Wu, *ACS Appl. Mater. Interfaces*, 2012, **4**, 1565.
18 J.-H. Kim, D.-H. Kim, K.-P. Kim, D.-H. Jeon and D.-K. Hwang, *Thin Solid Films*, 2013, **546**, 326.
19 J. Kim, J. K. Koh, B. Kim, J. H. Kim and E. Kim, *Angew. Chem., Int. Ed.*, 2012, **51**, 6864.

 

20 S. Wooh, H. Yoon, J.-H. Jung, Y.-G. Lee, J. H. Koh, B. Lee, Y. S. Kang and K. Char, *Adv. Mater.*, 2013, **25**, 3111.
21 J. Lee and M. Lee, *Adv. Energy Mater.*, 2014, **4**, 1300978.
22 Y. Shimotsuma, P. G. Kazansky, J. Qiu and K. Hirao, *Phys. Rev. Lett.*, 2003, **91**, 247405.
23 A. P. Joglekar, H. Liu, E. Meyhofer, G. Mourou and A. J. Hunt, *Proc. Natl. Acad. Sci. U. S. A.*, 2004, **101**, 5856.
24 M. Shen, J. E. Carey, C. H. Crouch, M. Kandyla, H. A. Stone and E. Mazur, *Nano Lett.*, 2008, **8**, 2087.
25 M. Farsari and B. N. Chichkov, *Nat. Photonics*, 2009, **3**, 450.
26 U. Zywietz, A. B. Evlyukhin, C. Reinhardt and B. N. Chichkov, *Nat. Commun.*, 2014, **5**, 3402.
27 R. R. Gattass and E. Mazur, *Nat. Photonics*, 2008, **2**, 219.
28 M. Huang, F. Zhao, Y. Cheng, N. Xu and Z. Xu, *ACS Nano*, 2009, **3**, 4062.
29 V. R. Bhardwaj, E. Simova, P. P. Rajeev, C. Hnatovsky, R. S. Taylor, D. M. Rayner and P. B. Corkum, *Phys. Rev. Lett.*, 2006, **96**, 057404.
30 J. Yoon, M. Jin and M. Lee, *Adv. Mater.*, 2011, **23**, 3974.